Acta Pharmacologica Sinica

www.nature.com/aps

ARTICLE

Silicone elastomer gel impregnated with 20(*S*)-protopanaxadiol-loaded nanostructured lipid carriers for ordered diabetic ulcer recovery

Di Sun[1], Shi-yan Guo[2], Li Yang[1], Ya-ru Wang[1], Xiao-hui Wei[1], Sha Song[2], Yi-wei Yang[2], Yong Gan[2] and Zheng-tao Wang[1]

Inefficient diabetic ulcer healing and scar formation remain a challenge worldwide, owing to a series of disordered and dynamic biological events that occur during the process of healing. A functional wound dressing that is capable of promoting ordered diabetic wound recovery is eagerly anticipated. In this study, we designed a silicone elastomer with embedded 20(*S*)-protopanaxadiol-loaded nanostructured lipid carriers (PPD-NS) to achieve ordered recovery in scarless diabetic ulcer healing. The nanostructured lipid carriers were prepared through an emulsion evaporation-solidification method and then incorporated into a network of silicone elastomer to form a unique nanostructured lipid carrier-enriched gel formulation. Interestingly, the PPD-NS showed excellent in vitro anti-inflammatory and proangiogenic activity. Moreover, in diabetic mice with full-thickness skin excision wound, treatment with PPD-NS significantly promoted in vivo scarless wound healing through suppressing inflammatory infiltration in the inflammatory phase, promoting angiogenesis during the proliferation phase, and regulating collagen deposition in the remodeling phase. Hence, this study demonstrates that the developed PPD-NS could facilitate ordered diabetic wound recovery via multifunctional improvement during different wound-healing phases. This novel approach could be promising for scarless diabetic wound healing.

Keywords: diabetic ulcer; ordered recovery; scarless wound healing; 20 (*S*)-protopanaxadiol; nanostructured lipid carrier; silicone elastomer

Acta Pharmacologica Sinica (2020) 41:119–128; https://doi.org/10.1038/s41401-019-0288-7

INTRODUCTION

Diabetic foot ulcers have been a major clinical challenge. The incidence of foot ulcers is ~25% in diabetic patients, and unfortunately, 14%–24% of these patients require amputation as a consequence of inefficient healing [1]. The healing process of diabetic ulcers involves three overlapping but gradual phases: inflammatory, proliferative, and remodeling [2], which are related to a series of complex and dynamic biological events. Any failures or defects in these biological events, such as excessive inflammatory cell infiltration, inefficient angiogenesis, or an imbalance of collagen synthesis and degradation, may influence the subtle equilibrium, resulting in disordered healing and scar complications. Unfortunately, inefficient healing and scarring always emerge in diabetic wounds in mammals, consequently causing psychological trauma, disfigurement, and loss of function.

Many bioactive scaffolds have been reported to achieve wound healing, e.g., chitosan–hyaluronic acid composite sponge scaffolds [3], collagen scaffolds [4], gelatin hydrogels [5], and dextran hydrogel scaffolds [6]. Most of these scaffolds serve as antimicrobial, antioxidant, anti-inflammatory, or proangiogenic dressings for enhanced tissue regeneration. These wound dressings can improve wound healing to some extent. However, focusing on a single mechanism may be insufficient to meet the requirements of the three gradual and complex biological processes of wound healing. Notably, it has been reported that early gestation fetal wounds can be healed scarlessly, with representative characteristics of neovasculature and dermal appendages, similar to normal skin. Compared with mammals, the key factors responsible for scarless embryonic healing involve reduced inflammatory cell infiltration in the inflammatory phase, a high content of hyaluronic acid that promotes angiogenesis in the proliferative phase and arrangement of collagen into a network in the remodeling phase [7, 8]. One of the major aglycones of dammarane-type tetracyclic triterpenoid saponins found in *Panax notoginseng* (Burk.) F. H. Chen, a medicinal herb widely used for the treatment of hemorrhage, blood stasis, bruises, swelling, and pain, is 20(*S*)-protopanaxadiol (PPD). Recently, PPD has been reported to be effective in diabetic wound healing due to its anti-inflammatory and pro-neovascularization activities [9, 10]. However, its low solubility has greatly limited its application. Therefore, a novel nanostructured lipid carrier (NLC) was used to embed PPD to increase its solubility and drug-loading (DL) efficiency. Silicone elastomer

[1]The MOE Key Laboratory of Standardization of Chinese Medicine and Shanghai Key Laboratory of Compound Chinese Medicines, Institute of Chinese Materia Medica, Shanghai University of Traditional Chinese Medicine, Shanghai 201203, China and [2]Shanghai Institute of Materia Medica, Chinese Academy of Sciences, Shanghai 201210, China
Correspondence: Zheng-tao Wang (ztwang@shutcm.edu.cn)
These authors contributed equally: Di Sun, Shi-yan Guo.

Received: 18 April 2019 Accepted: 11 July 2019
Published online: 18 September 2019

has been reported to be effective in wound healing and scar repair [11, 12]. Silicone elastomer is a crosslinked siloxane polymer with a three-dimensional network structure that has been reported to regulate collagen deposition through hydration [13, 14] and static electric field induction [15, 16] and therefore achieve scarless healing.

Based on the above-mentioned reasoning, we propose the concept of ordered recovery for scarless healing, which can ensure that the three wound phases proceed in accordance with the theoretical healing process, accelerating the wound healing process and simultaneously blocking the factors that may cause scars. To achieve ordered diabetic wound recovery, PPD-loaded nanostructured lipid carriers (PPD-NS) were prepared and dispersed in the three-dimensional network structure of a silicone elastomer. After careful characterization of in vitro anti-inflammatory and proangiogenic capacity and the in vivo inflammatory response, angiogenesis and collagen deposition were systematically evaluated. Owing to the synergistic effects of PPD-N particles and silicone elastomer in preventing inflammation, promoting angiogenesis, and regulating collagen deposition during the inflammatory, proliferative, and remodeling phases, respectively, ordered recovery was achieved during the healing process of diabetic ulcers, and the tissue was completely regenerated without scars. These results demonstrate that PPD-NS may qualify as a promising drug delivery system for scarless diabetic ulcer recovery.

MATERIALS AND METHODS

Materials

The 20(S)-PPD was provided by Shanghai R&D Center for Standardization of Chinese Medicines (purity > 98%, high-performance liquid chromatography (HPLC)). Silicone elastomer was kindly donated by Yuyu New Material Co., Ltd. (China). Glyceryl monostearate (GMS) was purchased from Hunan Ercan Pharmaceutical Co., Ltd. (China). Pluronic F-68 (F-68) was purchased from BASF (Germany). Medium-chain triglycerides (MCT) were acquired from GATTEFOSSé (France). HUVECs were obtained from ScienCell Research Laboratories (San Diego, CA, USA) and RAW264.7 cells were provided by the American Type Culture Collection (USA).

Preparation of the PPD-N and PPD-NS formulations

PPD-N was prepared through an emulsion evaporation-solidification method with modifications [17]. Briefly, PPD, GMS, and MCT were dissolved in anhydrous ethanol and heated to 85 °C, and the mixture was stirred at 85 °C for 30 min to remove the ethanol. Meanwhile, 5 mL of deionized water containing surfactant (Tween 80 and Pluronic F-68 at a ratio of 2:1) was heated to 85 °C. Then, the aqueous phase was added to the oil phase under mechanical shearing at 12000 r/min for 5 min to obtain the pre-emulsion. The pre-emulsion was further treated with a probe-type sonicator (Scientz-II D) at 30 W for 1 min, and the PPD-N dispersion was obtained.

PPD-NS was prepared by mixing silicone elastomer and the PPD-N dispersion at a ratio of 1:100 (w:w) [18] and stirring for 3 h to obtain a homogenous mixture.

Characterization of PPD-N and PPD-NS

The morphology, particle size, and zeta potential. The average particle size, polydispersity index (PDI), and zeta potential of the PPD-N particles and bare nanostructured lipid carriers were characterized using a ZetaSizer Nano ZS90 (Malvern Instruments Co., Ltd., Malvern, UK). The morphology of nanostructured lipid carriers after vacuum drying was observed by scanning electron microscopy (SEM, XL30, Philips). The silicone elastomer network was observed by cryo-scanning electron microscopy (Hitachi su8010).

Determination of encapsulation efficiency (EE) and DL. The EE and DL ability of PPD-N particles were detected using an ultrafiltration tube (MWCO 8 kDa) [19]. PPD-N dispersions were filtered to obtain free PPD and then assayed to obtain the amount of free PPD by an Agilent 1200 HPLC system (Agilent Technologies, Inc., Santa Clara, CA). The EE and DL abilities were calculated as follows:

$$\mathrm{EE}(\%) = \frac{W_t - W_f}{W_t} \times 100$$

$$\mathrm{DL}(\%) = \frac{W_t - W_f}{W_t - W_f + W_l} \times 100$$

where W_t is the initial drug amount, W_f is the free drug content in the ultrafiltrate, and W_L is the total lipid content.

Differential scanning calorimetry (DSC). DSC analysis was conducted to observe the structural organization state of the lipids [20]. Before measurements, nanostructured lipid carriers were lyophilized (PiloFD, Gold-Sim) and evaluated by DSC analysis (Q2000, NCC) at 25–150 °C with a heating rate of 10 °C/min.

In vitro release studies. A drug release study was performed with a dialysis bag [4]. Briefly, a dialysis bag (molecular cutoff of 8000–14 000) was prepared according to the instructions provided by Sigma. The release medium was 1 mM phosphate-buffered saline (PBS, pH 7.4) containing 5% Labrasol and 1% Tween 80. PPD-SOL (2 mL), PPD-N (2 mL), and PPD-NS (2 g), at the same concentration of 6 mg/mL (or 6 mg/g), were placed in dialysis bags and immersed in bottles containing 70 mL of the release medium. The bottles were capped and placed on a thermostatic shaker at 37 ± 0.5 °C and 100 r/min. Samples (1 mL) were taken at scheduled time intervals and evaluated by HPLC ($n = 3$).

Evaluation of anti-inflammatory activity in vitro. RAW264.7 cells were cultured in Dulbecco's modified Eagle's medium (DMEM) at 37 °C in a 5% CO_2 environment. To evaluate cell cytotoxicity, RAW264.7 cells were seeded into 96-well plates at a concentration of 3×10^4 cells/well, and 10 μM concentrations of the PPD formulations were applied for 24 h. Cell cytotoxicity was determined by 3-(4,5-dimethyl-2-thiazolyl)-2,5-diphenyl-2-H-tetrazolium bromide (MTT) [21].

To determine the NO content in the cell supernatant, RAW264.7 cells were seeded into 48-well plates (5×10^4 cells/well) and coincubated with PPD formulations (10 μM) for 2 h at 37 °C in a CO_2 incubator. Lipopolysaccharide (LPS, 100 ng/mL) was added to the culture and incubated for 22 h. The content of nitrite in the medium was measured using Griess reagent, which reflected the NO levels [22].

Evaluation of angiogenesis activity in vitro. HUVECs were cultured in DMEM at 37 °C in a 5% CO_2 environment. To evaluate cell viability, HUVECs were seeded into 96-well plates at a concentration of 5×10^3 cells/well, and 2.5 μM of PPD formulations were applied for 24 h. Cell viability was determined by MTT [21].

To detect cell migration activity, HUVECs were seeded in a 12-well plate (3.0×10^5 cells/well) and placed at 37 °C in a 5% CO_2 incubator. When the cell confluence reached 90%, scratches of the same width were made with a pipette tip and treated with 2.5 μM concentrations of PPD formulations for 24–48 h. Photos were taken under an inverted microscope and quantified with ImageJ software [23, 24].

To investigate the effect of PPD formulations on angiogenesis in vitro, HUVECs were seeded on Matrigel (BD Biosciences, USA), which was used to precoat a 96-well plate. The samples were incubated with the PPD formulations for 8 h. Tube networks were quantified by quantifying the number of nodes under an inverted microscope (Olympus CKX41, Tokyo, Japan) [25].

In vivo wound healing

Excisional wound splinting model. Twelve-week-old male mice (Lepr db/JNju, *db/db*) with hyperglycemia (27.3 ± 7.7 mM) were obtained from the Biomedical Research Institute of Nanjing University (Nanjing, China). All animal experiments were conducted in compliance with the Guide for the Care and Use of Laboratory Animals and the Institutional Animal Care guidelines approved by the Experimental Animal Ethical Committee of Shanghai University of Traditional Chinese Medicine. Full-thickness skin excision wounds (6 mm in diameter) were made according to the literature [26]. The animals were then divided into four groups: PBS, PPD suspension (PPD-S), PPD-N, and PPD-NS, with treatments locally delivered at the wound sites every 2 days in 15-μL or 15-mg doses. Wound appearance was recorded by a digital camera at different post-wounding time points and analyzed with ImageJ software.

$$\text{Wound closure percentage } (\%) = \frac{\text{area on day 0} - \text{area on day } n}{\text{area on day 0}} \times 100$$

Histological staining. The wound specimens were fixed in 4% paraformaldehyde and embedded in paraffin at different time intervals. Skin tissues were then examined through hematoxylin and eosin (H&E) staining, Masson's trichrome staining, and Sirius staining [27].

CD31 immunohistological staining. Angiogenesis in vivo was detected through CD31 immunohistological staining with the help of a rabbit anti-mouse CD31 antibody (Abcam) [28]. Images were obtained from four random fields and quantified with ImageJ software.

ELISA assay. The protein levels of TNF-α, IL-6, and CXCL5 in the inflammatory phase and VEGF in the proliferative phase at the wound sites were assayed by an ELISA kit (Sbjbio) according to the manufacturer's instructions [29, 30].

Statistical analysis. All data are presented as the mean ± standard deviation. Comparisons of different experimental groups were tested using two-way ANOVA followed by Tukey's multiple comparison test with GraphPad Prism 5.0. A value of $P < 0.05$ was defined as statistically significant.

RESULTS

Characterization of PPD-N and PPD-NS

PPD-N was prepared through the emulsion evaporation-solidification method. The basic properties of bare and PPD-loaded NLC formulations are listed in Table 1. The particle sizes of PPD-N (111.4 ± 5.9 nm) were higher than those of the bare formulations (99.2 ± 5.5 nm). The PDI was ~0.2 for both formulations. The surface of the NLC was surrounded by negative charges, and the absolute value was close to 30 mV. In addition, the EE of PPD-N was as high as 97.9% ± 1.51%, with DL percentages up to 9.8% ± 0.29%.

The morphology of the NLC (Fig. 1a) indicated spherical, uniformly distributed nanometer-sized particles, consistent with the results measured by ZetaSizer (Fig. 1b). Field emission cryo-scanning electron microscopy images are shown in Fig. 1c. The appearance of silicone elastomer suggested an interconnected porous architecture with apertures ranging from 300 to 600 nm in size. The images of PPD-NS showed the homogeneous distribution of PPD-N particles throughout the silicone elastomer network.

Table 1. Particle size distribution, zeta potential, and entrapment efficiency of PPD-N and bare N ($n = 3$)

Content	*Z* average	PDI	Zeta	EE (%)	DL (%)
Bare N	99.2 ± 5.5	0.16 ± 0.07	−34.8 ± 4.0	/	/
PPD-N	111.4 ± 5.9	0.21 ± 0.04	−33.2 ± 5.5	97.9 ± 1.51	9.8 ± 0.29

DSC analysis (Fig. 1d) showed that the thermograms of GMS and F-68 showed a specific endothermic melting peak at ~60 °C and 51 °C, respectively. There were no obvious changes in the physical mixture, while the melting peak of GMS significantly decreased and the dissolution temperature decreased from 60 °C to 52 °C in the lyophilized NLC.

In vitro release profiles are shown in Fig. 1e. The release curve from PPD-N and PPD-NS demonstrated a biphasic trend characterized by rapid release for the initial 24 h, accompanied by a sustained-release phase. In 24 h, 90.74% ± 3.23% of the PPD was released from PPD-SOL. From PPD-N and PPD-NS, 60.65% ± 2.47% and 42.11% ± 1.24% of the PPD, respectively, became available. In 72 h, 93.40% ± 1.61% of the PPD became available from PPD-SOL. The accumulated amount of PPD released from PPD-NS was ~72.92% ± 2.02%, which was significantly lower than that of PPD-N (85.84% ± 2.39%).

Anti-inflammatory potential in vitro

Prior to the evaluation of anti-inflammatory activities, the cytotoxicity of PPD formulations in RAW264.7 cells was examined by an MTT assay. Fig. 2a shows that there was no significant difference in cell viability at concentrations of 5 and 10 μM, while cell viability decreased to 63.35% ± 2.75% after treatment with 20 μM, suggesting that PPD formulations at 10 μM had no significant cytotoxic effect on RAW264.7 cells. Accordingly, formulations at a concentration of 10 μM were selected for continuing the following experiments.

To determine the anti-inflammatory potential of the formulations, the level of NO in the cell supernatant was detected using Griess reagent. The results showed that the NO levels in RAW264.7 cells remarkably increased under stimulation with LPS ($P < 0.001$). However, pretreatment with PPD formulations could obviously reduce the NO level (Fig. 2b). Compared with PPD-SOL, there was significant NO inhibition with PPD-N ($P < 0.01$) and PPD-NS ($P < 0.05$), indicating their good anti-inflammatory potential.

Angiogenesis activity in vitro

Our previous work suggested that PPD at 2.5 μM had good proangiogenic capacity by promoting the secretion of VEGF, which enhanced tissue regeneration [9]. Therefore, in vitro angiogenesis, cell proliferation, and migration assays were conducted to test the proangiogenic ability of PPD formulations. As shown in Fig. 3a, HUVECs in the PPD-treated groups formed integrated network structures on the Matrigel after 8 h. Compared with that in cells treated with PPD-SOL, there was a significant increase in the number of tubes in cells treated with PPD-N ($P < 0.05$), especially in the PPD-NS groups ($P < 0.05$), which possessed the most tubes (Fig. 3c).

In addition, cell proliferation and migration were investigated. Compared with that in the PPD-SOL group, cell viability in the PPD-N group was significantly enhanced ($P < 0.05$), while there was no significant difference compared with the PPD-NS group (Fig. 3d). The cell migration results are shown in Fig. 3b. Initially, scratches of the same width were made on the bottom of each well, and the scratched wound area was obviously reduced in 24 h, especially after incubation with PPD-N ($P < 0.05$) and PPD-NS ($P < 0.01$). At 48 h, the scratched area was almost closed in the PPD-NS group, while the closure rate was only 56.89% ± 5.81% in the PPD-SOL group (Fig. 3e).

In vivo wound healing

PPD-NS promoted ordered diabetic ulcer healing. To assess the wound healing potential of PPD-NS, in vivo pharmacodynamic

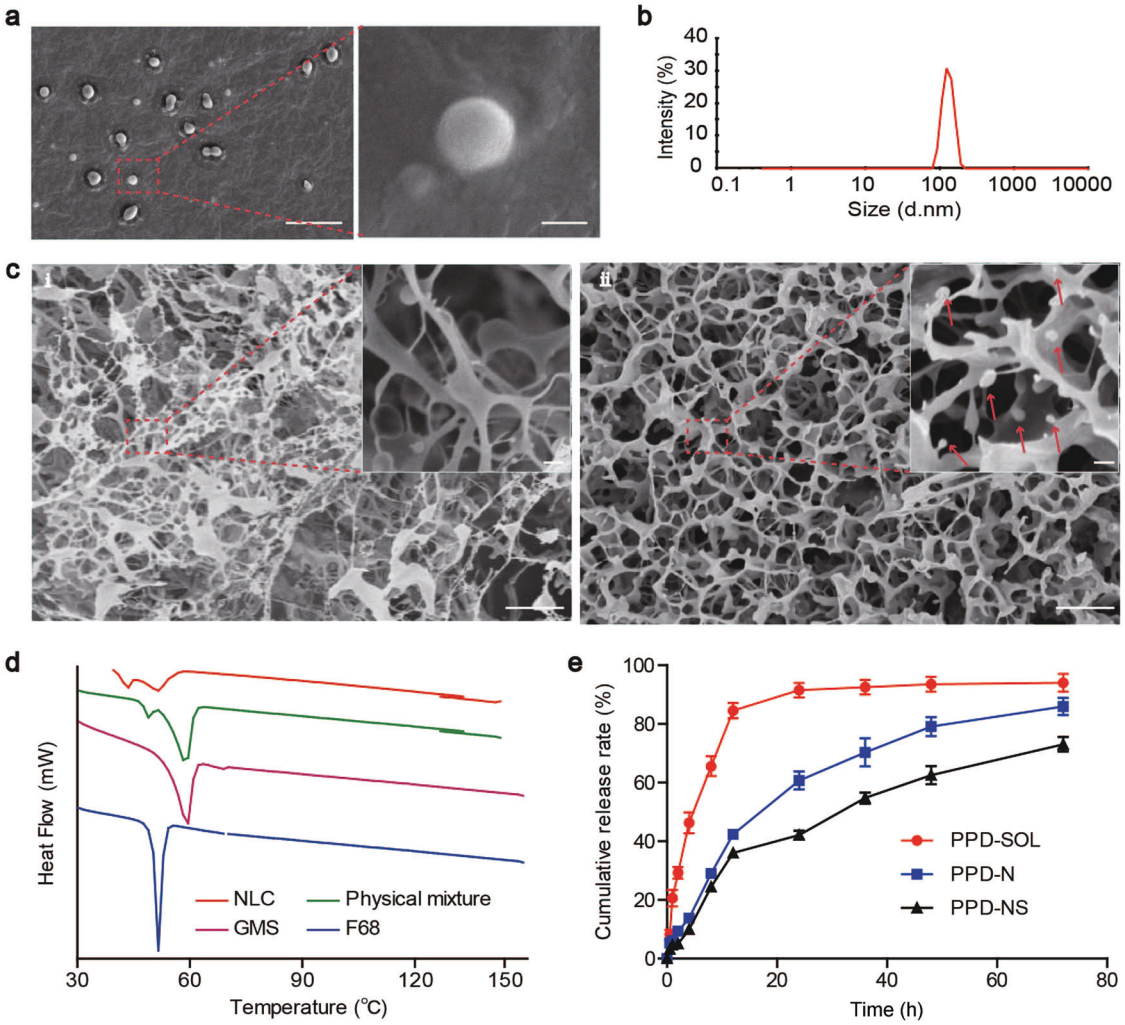

Fig. 1 Formulation characterization. **a** SEM images of PPD-N; scale bars, 50 and 500 nm. **b** Particle size of PPD-N. **c** Fro-SEM images of (i) silicone elastomer without nanostructured lipid carriers and (ii) silicone elastomer impregnated with nanostructured lipid carriers; scale bars, 200 nm and 2 μm. **d** DSC thermograms of GMS, F-68, the physical mixture, and the NLC formulation. **e** In vitro release profile of PPD from PPD-SOL, PPD-N, and PPD-NS ($n = 3$)

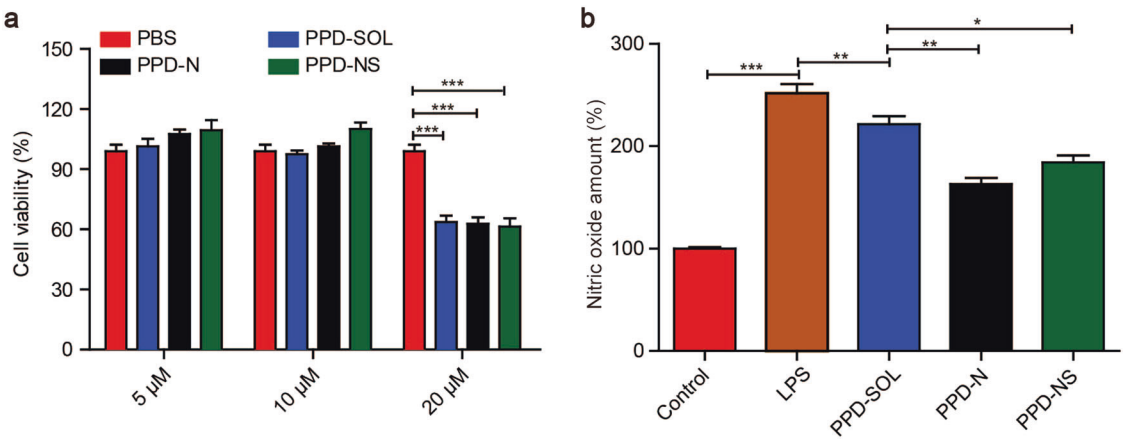

Fig. 2 Characterization of anti-inflammatory activity in vitro. **a** Cytotoxicity of PPD formulations in RAW264.7 cells treated with PPD formulations for 24 h. **b** NO level in RAW264.7 cells. The LPS-treated group was included as a control. $^{*}P < 0.05$, $^{**}P < 0.01$, $^{***}P < 0.001$

evaluation was carried out on *db/db* diabetic mice with excisional wounds. As shown in Fig. 4a, the cumulative wound contraction rate of the PPD-NS-treated group (98.18% ± 3.07%, $P < 0.01$) was significantly higher than that of the PBS (71.67% ± 12.4%) and PPD-S (86.52% ± 9.92%) groups. However, there was no significant difference compared with the PPD-N-treated groups (94.72% ± 6.48%) (Fig. 4c). Wounds in the PPD-NS group were fully closed without scars, native to unwounded tissue, while there were scars

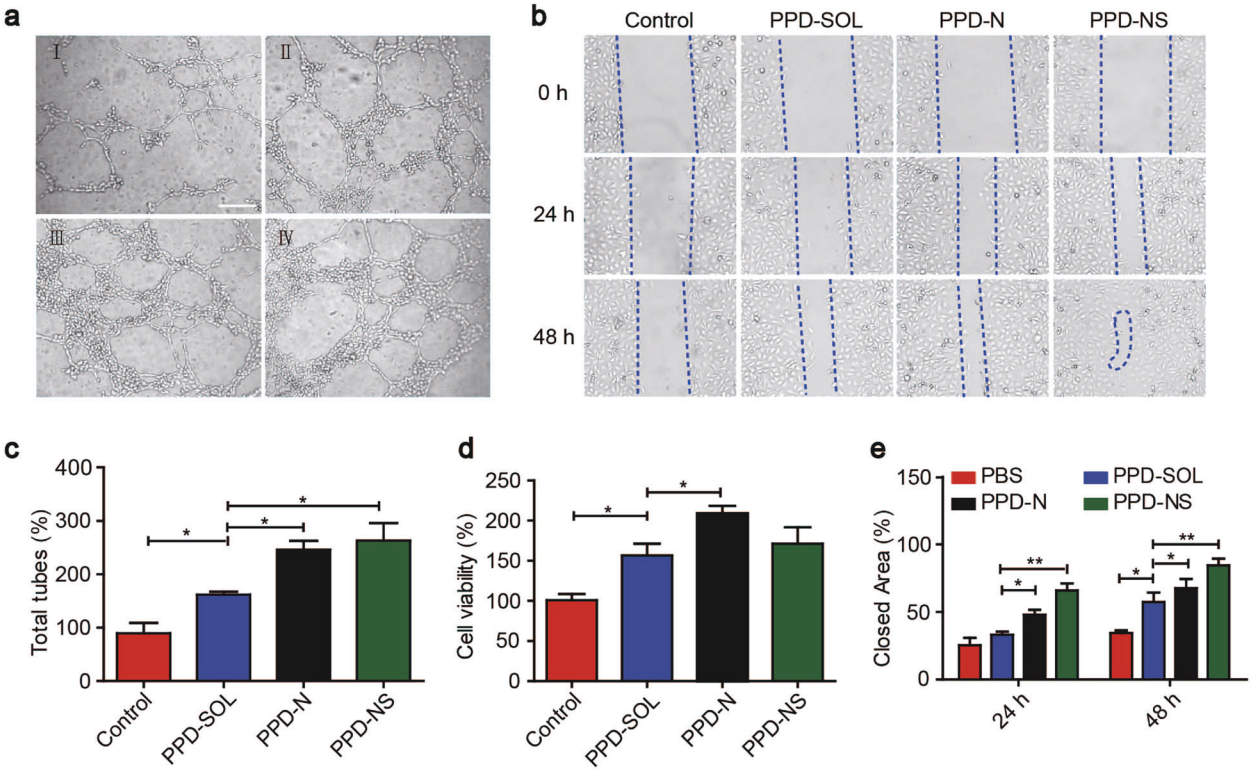

Fig. 3 Characterization of proangiogenic activity in vitro. **a** Angiogenesis of HUVECs incubated with the control (I), PPD-SOL (II), PPD-N (III), and PPD-NS (IV). Scale bars, 250 μm. **b** Representative images of the migration of HUVECs. **c** Quantitative analysis of tube nodes in each field. **d** Cell viability after treatment with PPD formulations. **e** Quantitative analysis of the migration rate by ImageJ software. $^{*}P < 0.05$, $^{**}P < 0.01$

in the PPD-N group (as indicated by a yellow arrow). These wound closure rates matched well with the results of the wound scratch assay in vitro.

Tissue specimens at different time intervals were evaluated by H&E staining (Fig. 4b). Statistical analysis demonstrated that the epithelial gap in the PPD-N and PPD-NS groups narrowed significantly faster than that in the PPD-S group at 14 and 21 days (Fig. 4d). Granulation tissue formed gradually at the wound site and filled the wound lesion completely on the 21th day in the PPD-NS group, while there were fewer granulation tissues in the PPD-S group (Fig. 4e). Tissue staining results analyzed by ImageJ software were consistent with the microscopy study.

PPD-NS suppressed inflammation in the inflammatory phase. Specimens at days 3 and 7 were analyzed by H&E staining (Fig. 5a). Compared with that in the PBS group, the number of inflammatory cells was reduced in all PPD-treated groups. Compared with PPD-S, there was a significant reduction of inflammatory cells in the PPD-N ($P < 0.05$) and PPD-NS groups ($P < 0.01$) at day 7 (Fig. 5b).

According to the literature, reductions in proinflammatory cytokines [31, 32] and chemokines [33, 34] are important indicators for evaluating the regression of inflammation. Thus, the concentrations of proinflammatory cytokines (TNF-α and IL-6) and chemokines (CXCL5) were determined with ELISA kit, and the samples were prepared from the animal wound tissues on day 7. As a result, compared with PPD-S, treatment with PPD-NS showed significant inhibition of inflammation responses by reducing the levels of TNF-α, IL-6, and CXCL5 (Fig. 5c–e: TNF-α, PPD-S: 628.53 ± 30.40 pg/mL; PPD-NS: 480.02 ± 15.00 pg/mL; PPD-S vs PPD-NS: $P < 0.001$; IL-6, PPD-S: 108.86 ± 4.84 pg/mL; PPD-NS: 61.36 ± 3.20 pg/mL; PPD-S vs PPD-NS: $P < 0.001$; CXCL5, PPD-S: 3536.02 ± 169.83 pg/mL; PPD-NS: 2653.84 ± 156.00 pg/mL; PPD-S vs PPD-NS: $P < 0.01$).

PPD-NS promoted angiogenesis in the proliferative phase. Specimens at days 7, 14, and 21 were analyzed by CD31 immunohistological staining (Fig. 6a). The results revealed negligible newly formed blood vessels in the PBS group, and small blood vessels (indicated by red arrows) were observed in the PPD-S group. In comparison, an increasing number of blood vessels were formed in the PPD-N groups, especially in the PPD-NS group (Fig. 6b). Simultaneously, compared with PPD-S, the protein levels of VEGF in the PPD-N group were significantly increased (Fig. 6c: VEGF at day 14, PPD-S: 200.34 ± 16.14 pg/mL; PPD-NS: 270.95 ± 11.10 pg/mL; PPD-S vs PPD-NS: $P < 0.001$; VEGF at day 21, PPD-S: 207.83 ± 18.72 pg/mL; PPD-NS: 240.33 ± 4.38 pg/mL; PPD-S vs PPD-NS: $P < 0.001$).

PPD-NS regulated collagen deposition in the remodeling phase. Masson's trichrome staining was used to examine collagen deposition. As shown in Fig. 7a, the collagen content of the wound region gradually increased at different time intervals. Compared with the PPD-S group, there was more collagen deposited in the PPD-N ($P < 0.01$) and PPD-NS ($P < 0.05$) groups at 21 days (Fig. 7b). Moreover, the collagen deposited in the PPD-NS group had a multiangle orientation, generating a whirled reticular status with obvious skin appendages. Conversely, collagen was flat against and parallel to the epidermis devoid of skin appendages with characteristics of scars in the PPD-N group. The collagen fibrils were loosely arranged and irregular in the PBS and PPD solution groups.

Sirius staining was used to distinguish between type I and type III collagen; type I collagen was stained yellow/red, and type III collagen was stained green. From Fig. 7c, there was gradually enhanced green fluorescence intensity in the PPD-NS group, while substantial red/yellow fluorescence was observed in the PPD-N and PPD-S groups, revealing that there was a lower ratio of type I/III collagen in the PPD-NS group. The relative proportion of type

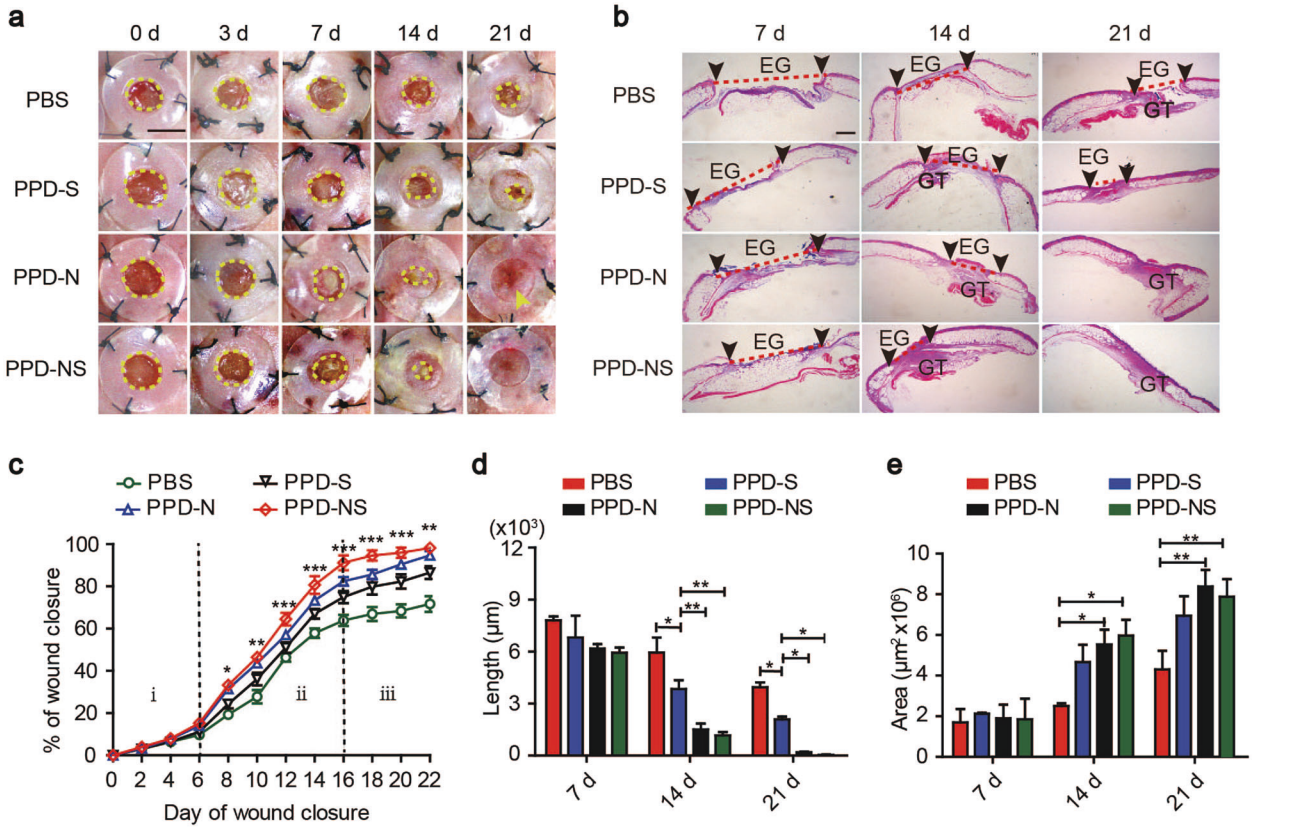

Fig. 4 In vivo wound healing efficacy. **a** Wound appearance after treatment with different formulations. Arrows indicate scars. Scale bars, 6 mm. **b** Microphotographs of H&E-stained wound specimens. Scale bars, 1 mm. **c** Quantitative analysis of the cumulative healing rate in different phases: inflammatory (i), proliferative (ii), and remodeling (iii). **d**, **e** Measurements of epithelial gap length (EG) and granulation tissue area (GT). $^{*}P < 0.05$, $^{**}P < 0.01$, $^{***}P < 0.001$

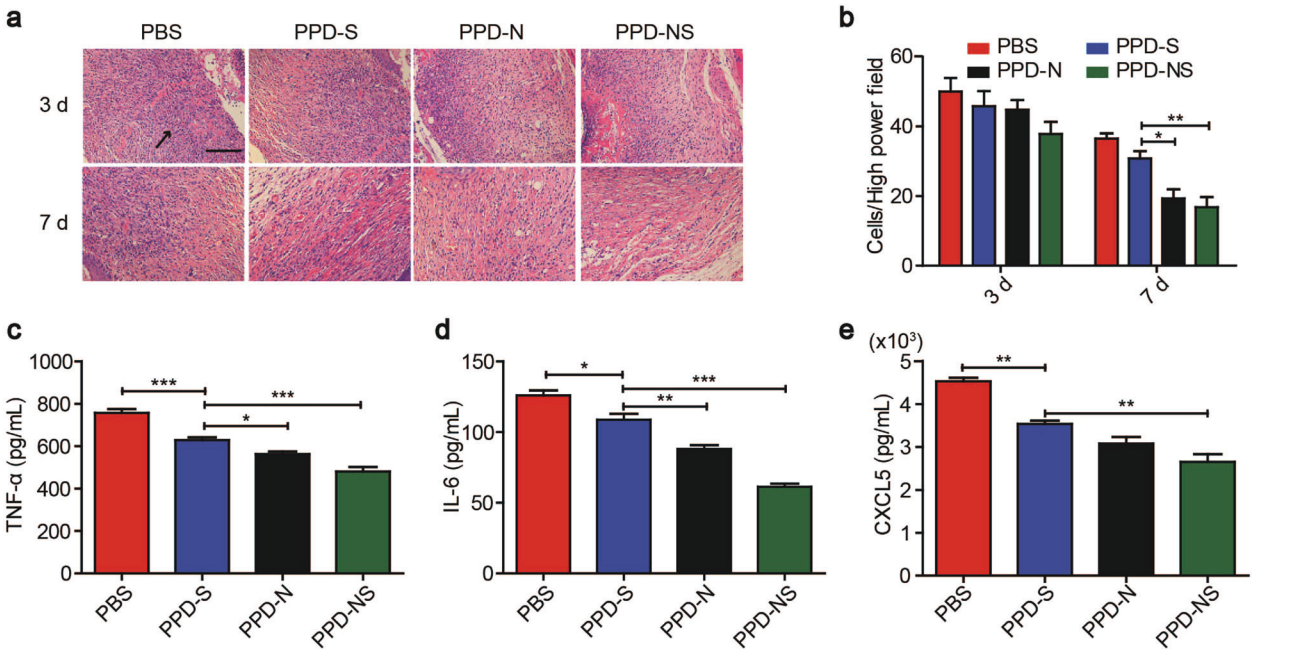

Fig. 5 In vivo anti-inflammatory efficacy. **a** Images of inflammatory cell infiltration at the wound sites. Arrows indicate inflammatory cells. Scale bars, 250 μm. **b** Quantitative analysis with ImageJ software. **c**–**e** Effect of PPD formulations on the levels of TNF-α, IL-6, and CXCL5 in wounds at day 7. $^{*}P < 0.05$, $^{**}P < 0.01$, $^{***}P < 0.001$

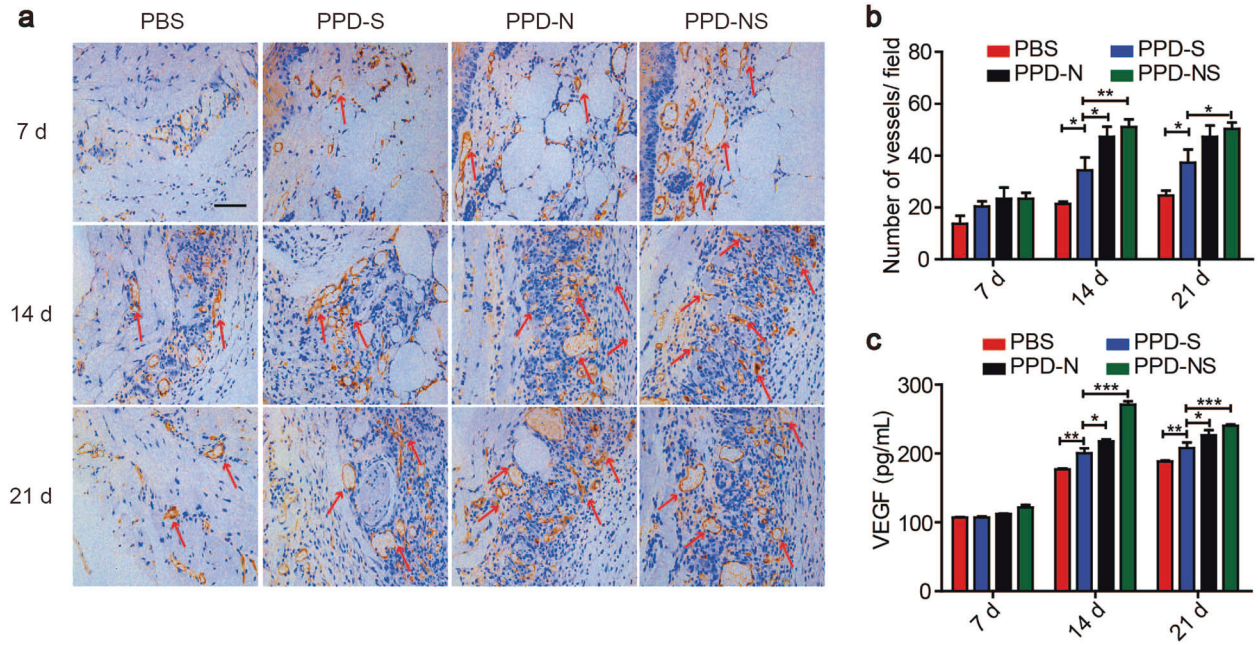

Fig. 6 In vivo proangiogenic efficacy. **a** IHC staining with CD31. Arrows indicate newly formed blood vessels. Scale bars, 250 μm. **b** Quantitative analysis of angiogenesis. **c** Effect of PPD formulations on the level of VEGF in wounds at days 7, 14, and 21. $^{*}P < 0.05$, $^{**}P < 0.01$, $^{***}P < 0.001$

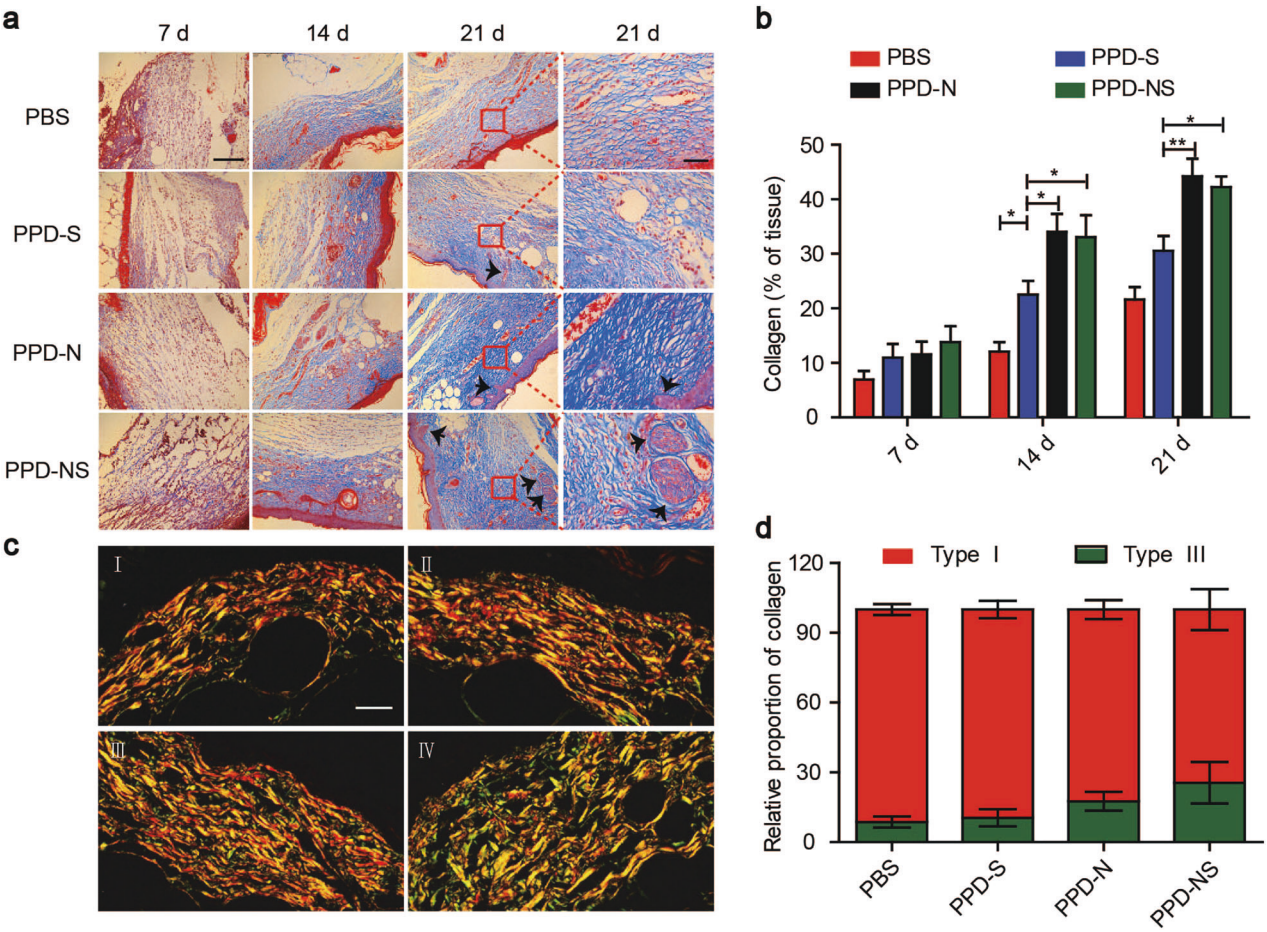

Fig. 7 In vivo collagen regulation efficacy. **a** Collagen deposition at wound sites. Arrows indicate skin appendages. Scale bars, 250 and 100 μm. **b** Quantitative analysis of collagen content with ImageJ software. **c** Sirius red staining at 21 days post wounding in the groups treated with PBS (I), PPD-S (II), PPD-N (III), and PPD-NS (IV). Scale bars, 100 μm. **d** Relative proportion of type I/type III collagen. $^{*}P < 0.05$, $^{**}P < 0.01$

I/III collagen in each group is shown in Fig. 7d, which was consistent with the results observed under the microscope.

DISCUSSION

Diabetic ulcers are healed by a complex biological process that involves three overlapping but gradual phases: inflammatory, proliferative, and remodeling [2]. Any disruption of biological balance, such as excessive inflammation, inefficient angiogenesis, or abnormal collagen deposition may lead to a series of disordered and complicated biological events, ultimately resulting in inefficient diabetic ulcer healing and scar formation. Many wound dressings have been reported for wound healing and scar repair. Most of these dressings serve as antimicrobial, anti-inflammatory, proangiogenic, or collagen-regulatory dressings for enhanced tissue regeneration. However, focusing on a single mechanism is insufficient to achieve functional tissue regeneration. Herein, a composite mechanism involving the synergy of PPD-NS was proposed, which inhibited inflammation in the inflammatory phase, promoted angiogenesis in the proliferative phase, and regulated collagen deposition in the remodeling phase, achieving ordered recovery for efficient scarless healing.

In this research, silicone elastomer impregnated with 20(*S*)-PPD-NS was designed for a synergistic effect to achieve ordered diabetic ulcer recovery. Nanostructured lipid carriers were prepared through an emulsion evaporation-solidification method and then incorporated into a network of silicone elastomer to achieve synergy. Our previous work indicated that PPD has good anti-inflammatory and pro-neovascularization activities [9, 10], which could be effective in the inflammatory and proliferative phases, accelerating diabetic ulcer healing. In addition, silicone elastomer, a lightly crosslinked polymer with excellent physical and chemical properties, has been reported for wound healing and scar repair [11, 12]. The mechanisms are mainly related to the hydration [13, 14] and electrostatic field effects [15, 16]. If the wound site is dehydrated, the stratum corneum wound immediately signals to keratinocytes to produce inflammatory cytokines, which subsequently send a signal to fibroblasts to synthesize and secrete excessive amounts of collagen for water retention at wound sites. This process is the cause of undesirable scars. The application of silicone elastomer could replicate the stratum corneum's occlusion properties and provide improved hydration in the wound bed, which in turn inhibits cytokines, fibroblast activity, and collagen formation. Moreover, inhibition of the secretion of inflammatory cytokines could shorten the length of the inflammatory phase and promote wound healing. In addition, it has been reported that the electrostatic effect of silicone elastomers can regulate the alignment of collagen fibers and inhibit scar formation in the remodeling phase during the wound healing process.

The characterization results are shown in Table 1 and Fig. 1. According to the literature, the particle size obtained was suitable for ensuring nanoparticle adherence and local delivery to the wound site [35]. The PDI was ~0.2 for both PPD-N and the bare formulations, indicating a narrow, monodispersed distribution. The negative charges on the surface of the NLC provided formulations with good stability [36]. The results of EE and DL percentages indicated that the PPD-NS has a good DL capacity, which are essential parameters in terms of drug delivery.

DSC analysis was performed to explore the crystallization changes of the lipids. The changes in thermograms between the physical mixture and the lyophilized NLC indicated that GMS in the NLC was amorphous or imperfect crystalline. Due to the presence of liquid lipids, the structure of solid lipids was destroyed, and there was a subsequent increase in amorphous or imperfect lipids, consequently generating more free spaces to entrap drugs [37].

The cryo-SEM images of silicone elastomer suggested an interconnected porous architecture with apertures ranging from 300 to 600 nm in size, which was preferable for cell proliferation and migration for wound healing. Moreover, this network could serve as a barrier against bacteria entering the wound site, accelerating wound healing. The images of PPD-NS confirmed that PPD-N was in an integral particle structure and homogeneously distributed throughout the network of silicone elastomer, which was of great importance for achieving a synergistic effect on tissue regeneration.

To simulate the release behavior of PPD-NS at the wound site, the in vitro release profile was monitored. According to the literature, the pH of wound fluids is ~7–8 [28]. Thus, PBS buffer containing 1% Tween 80 and 5% Labrasol (pH 7.4) was chosen as the release medium. The release curve from PPD-N and PPD-NS demonstrated a biphasic trend characterized by rapid release in 24 h and a sustained-release phase. The burst release could be attributed to the presence of liquid lipids that caused a small particle size with increased surface area [38]. In addition, the cumulative amount of PPD released from PPD-NS was lower than that from PPD-N, which might result from the sequential release mechanism of PPD in PPD-NS, in which PPD-N diffused through the porous structure of the silicone elastomer first and then PPD diffused through the NLC. Both the rapid and sustained-release profiles were significant for wound healing, as the former ensured a sufficient dose to accelerate healing, while the latter process provided additional drugs in a continuous manner during the entire healing period.

Inhibition of inflammatory cell infiltration in the inflammatory phase and promotion of angiogenesis in the proliferative phase are key factors in achieving ordered diabetic ulcer recovery for scarless wound healing. In vitro evaluation results of anti-inflammation potential and angiogenesis activity are shown in Figs. 2 and 3. Compared with that in the PPD-SOL group, the significant NO inhibition in the PPD-NS group indicated good anti-inflammatory potential for accelerating wound healing. Angiogenesis is a process of new capillary network formation facilitated by the proliferation and migration of vascular endothelial cells [39]. The largest number of blood vessels in the PPD-NS groups suggested good pro-angiogenesis activity, which might be ascribed to the synergistic effect of PPD-N and silicone elastomer. Continuously released from the network of silicone elastomer, PPD-N particles were internalized into HUVECs, stimulated VEGF secretion, and ultimately promoted angiogenesis. Simultaneously, owing to the porous structure, the silicone elastomer acted as a scaffold for cell proliferation and migration, which facilitated vascular regeneration. Both the anti-inflammatory and proangiogenic activities of PPD-NS were the basis for achieving ordered recovery in vivo.

To further assess ordered diabetic ulcer healing, in vivo pharmacodynamic evaluation was carried out on *db/db* diabetic mice with excisional wounds. As observed in Fig. 4c, initially, the healing rate was slow, indicating that the wound site was in a state of inflammation. Subsequently, an evident increase in the average healing rate suggested that the wound transitioned into a proliferative phase. Then, the healing rate decreased again in a final remodeling period. In the PPD-NS group, the three wound phases proceeded normally in accordance with the theoretical healing process, which indicated that ordered diabetic wound recovery was achieved.

In the inflammatory phase, the number of inflammatory cells and the levels of proinflammatory cytokines (TNF-α and IL-6) and chemokines (CXCL5) were obviously reduced in the PPD-NS groups at day 7, suggesting that inflammation was significantly inhibited. This effect might be ascribed to the synergistic healing effect of PPD-NS. Initially, PPD-N was rapidly released from the porous structure of the silicone elastomer, and a large amount of PPD-N accumulated at the inflammatory wound site in a short time. Many PPD-N particles were immediately engulfed by inflammatory cells in the inflammatory phase to inhibit inflammatory factor expression, synergistic with the function of the

silicone elastomer to indirectly inhibit inflammation through hydration, successfully transitioning the wound into the proliferative phase.

During the proliferative phase, PPD-N particles underwent sustained and continuous release from the silicone elastomer network and were internalized by HUVECs to stimulate VEGF secretion and promote angiogenesis, exerting a synergistic effect with the silicone elastomer, which acted as a scaffold for HUVEC migration to accelerate blood vessel regeneration. As a consequence, many blood vessels were observed in the regenerated tissue treated with PPD-NS, while negligible newly formed blood vessels formed in the PBS and PPD-S groups. Correspondingly, the protein levels of VEGF in the PPD-NS group were obviously higher than those in the PPD-S group in the proliferative phase, demonstrating the excellent proangiogenic capability in the PPD-NS group due to the synergistic effect. Newly formed blood vessels could benefit wound healing remarkably because of the oxygen and nutrients they supply to the granulation tissue [40]. These vessels could serve as bridges for cells in the blood to migrate to the wound sites and adjust wound regeneration.

When almost closed, the wounds transitioned into the remodeling phase. The silicone elastomer present at the wound site formed a thin film that provided a level of hydration and indirectly inhibited the synthesis of collagen. Meanwhile, the static electric field generated between the silicone elastomer and the new epidermis regulated the orientation of collagen, which effectively attenuated scars. The orientation of collagen fibers is a key factor in evaluating scars because of the different mechanical forces produced by different arrangements. In previous studies, collagen with a uniform orientation always generated a strong contraction force and resulted in scar formation, which was harmful to the growth of skin appendages in the epidermis [41, 42]. The collagen deposited in the PPD-NS group had a multiangle orientation with obvious skin appendages, suggesting complete regeneration of the tissue. In addition, the collagen composition is also an important factor in evaluating the wound healing effect. According to the literature, both type III collagen and type I collagen can support the extracellular matrix and facilitate wound healing. However, excessive secretion of type I collagen might result in a disordered fiber structure and scar formation. Therefore, a low ratio of type I/III collagen content was indicative of improved regeneration [43]. There was a lower ratio of type I/III collagen in the PPD-NS group, indicating a scarless diabetic ulcer healing effect due to synergy in the PPD-NS group.

Overall, due to the synergistic effects of different properties of PPD-N and silicone elastomer, the developed PPD-NS facilitated ordered diabetic ulcer recovery via multifunctional improvement during the three important wound-healing phases, ultimately achieving scar-free healing.

CONCLUSION

In this research, silicone elastomer impregnated with 20(*S*)-PPD-NS was designed with good EE, DL efficiency, and sustained-release properties. This formulation exhibited excellent anti-inflammatory and proangiogenic capacity in vitro, and ordered wound recovery was successfully achieved in vivo through suppression of inflammatory infiltration, promotion of angiogenesis, and regulation of collagen during the inflammatory, proliferative, and remodeling phases, respectively. Owing to the synergistic effect of PPD-N and silicone elastomer in each healing phase, PPD-NS could be a promising candidate for scarless diabetic wound healing.

ACKNOWLEDGEMENTS

This work was financially supported by the National Natural Science Foundation of China (81530096 and 81573588).

AUTHOR CONTRIBUTIONS

ZTW and YG designed the research. DS, SYG, LY, YRW, XHW and SS performed the research. DS and SYG analyzed the data. DS, SYG, YWY, YG, and ZTW wrote the paper. All authors approved the final paper.

ADDITIONAL INFORMATION

Competing interests: The authors declare no competing interests.

REFERENCES

1. Sekhar MS, Unnikrishnan MK, Vijayanarayana K, Rodrigues GS, Mukhopadhyay C. Topical application/formulation of probiotics: will it be a novel treatment approach for diabetic foot ulcer? Med Hypotheses. 2014;82:86–8.
2. Pratsinis H, Mavrogonatou E, Kletsas D. Scarless wound healing: from development to senescence. Adv Drug Deliv Rev. 2018. https://doi.org/10.1016/j.addr.2018.04.011.
3. Basset Sanad RA, AbdelBar HM. Chitosan-hyaluronic acid composite sponge scaffold enriched with andrographolide-loaded lipid nanoparticles for enhanced wound healing. Carbohydr Polym. 2017;173:441–50.
4. ReddyKarri VVS, Kuppusamy G, Venkata Talluri SV, Mannemala SS, Kollipara R, Wadhhwani AD, et al. Curcumin loaded chitosan nanoparticles impregnated into collagen- alginate scaffolds for diabetic wound healing. Int J Biol Macromal. 2016;93:1519–29.
5. Notodihardjo PV, Morimoto N, Kakudo N, Matsui M, Sakamoto M, Liem PH, et al. Gelatin hydrogel impregnated with platele-rich plasma releasate promotes angiogenesis and wound healing in murine model. J Tissue Eng Regen Med. 2015;18:64–71.
6. Sun GM, Zhang XJ, Shen YI, Sebastian R, Dickinson LE, Talbot KF, et al. Dextran hydrogel scaffolds enhance angiogenic responses and promote complete skin regeneration during burn wound healing. Proc Natl Acad Sci USA. 2011;8:20976–81.
7. Keane TJ, Maria Horejs C, Stevens MM. Scarring vs. functional healing: matrix-based strategies to regulate tissue repair. Adv Drug Deliv Rev. 2018;129:407–19.
8. Wang PH, Huang BS, Horng HC, Yeh CC, Chen YJ. Wound healing. J Chin Med Assoc. 2018;81:94–101.
9. Zhang EY, Gao B, Shi HL, Huang LF, Yang L, Wu XJ, et al. 20(S)-Protopanaxadiol enhances angiogenesis via HIF-1-mediated VEGF secretion by activating p70S6 kinase and benefits wound healing in genetically diabetic mice. Exp Mol Med. 2017;49:1–11.
10. Lee YJ, Han JY, Lee CJ, Heo k, Park S, Park YS, et al. Korean red ginseng saponin fraction modulates radiation effects on lipopolysaccharide-stimulated nitric oxide production in RAW264.7 macrophage cells. J Ginseng Res. 2014; 38:208–14.
11. Palefsky I, Wilson N. Silicone gel-based compositions for wound healing and scar reduction. America:US8859618B2; 14 Oct 2014.
12. Wang YW, Beekman J, Hew J, Jackson S, IsslerFisher AC, Parungao R, et al. Burn injury: challenges and advances in burn wound healing, infection, pain and scarring. Adv Drug Deliv Rev. 2018;123:3–17.
13. Bleasdale B, Finnegan S, Murray K, Kelly S, Percival SL. The use of silicone adhesives for scar reduction. Adv Wound Care. 2015;4:422–30.
14. Xu R, Luo GX, Xia HS, He WF, Zhao J, Liu B, et al. Novel bilayer wound dressing composed of silicone rubber with particular micropores enhanced wound re-epithelialization and contraction. Biomaterials. 2015;40:1–11.
15. Borgognoni L. Biological effects of silicone gel sheeting. Wound Repair Regen. 2010;10:118–21.
16. Hirshowitz B, Lindenbaum E, Har-Shai Y, Feitelberg L, Tendler M, Katz D. Static-electric field induction by a silicone cushion for the treatment of hypertrophic and keloid scars. Plast Reconstr Surg. 1998;101:1173–83.
17. Fathi HA, Allam A, Elsabahy M, Fetih G, EiBadry M. Nanostructured lipid carriers for improved oral delivery and prolonged antihyperlipidemic effect of simvastatin. Colloid Surf B. 2018;1:236–45.
18. Dow Corning. Topical excipients formulation guide. www.Dowcorning.com/healthcare. 2007.
19. Mohan A, Rajendran SR, Thilbodeau J, Bazinet L, Udenigwe CC. Liposome encapsulation of anionic and cationic whey peptides: influence of peptide net charge on properties of the nanovesicles. LWT-Food Sci Technol. 2018;87:40–6.
20. Drzeżdżon J, Jacewicz D, Sielicka S, Chmurzyński L, EiBadry M. Characterization of polymers based on differential scanning calorimetry based techniques. Tractrend Anal Chem. 2019;110:51–6.
21. Zhan Gao, Wang H, Xiao FJ, Zhang YK, Xu QQ, Zhang XY, et al. SIRT1 mediates Sphk1/ S1P-induced proliferation and migration of endothelial cells. Int J Biochem Cell B. 2016;74:152–60.

22. Hwang JH, Kim KJ, Ryu SJ, Lee BY. Caffeine prevents LPS-induced inflammatory responses in RAW264.7 cells and zebrafish. Chem-Biol Interact. 2016;248:1–7.
23. Enomoto S, Mitsui K, Kawamura T, Lwamari H, Daigo K, Horiuchi K, et al. Suppression of Slit2/Robo1 mediated HUVEC migration by Robo4. Biochem Biophys Res Commun. 2016;469:797–802.
24. Nikhil K, Sharan S, Wishard R, Palla SR, Krishna PR, Roy P. Pterostilbene carboxaldehyde thiosemicarbazone, a resveratrol derivative inhibits 17beta-Estradiol induced cell migration and proliferation in HUVECs. Steroids. 2016;108:17–30.
25. Liu P, Li XS, Song FU, Li P, Wei JZ, Yan Q, et al. Testosterone promotes tube formation of endothelial cells isolated from veins via activation of Smad1 protein. Mol Cell Endocrinol. 2017;446:21–31.
26. Wang XS, Ge JF, Tredget EE, Wu YJ. The mouse excisional wound splinting model, including applications for stem cell transplantation. Nat Protoc. 2013;8:302–9.
27. Shamloo A, Sarmadi M, Aghababaie Z, Vossoughi M. Accelerated full-thickness wound healing via sustained bFGF delivery based on a PVA/chitosan/gelatin hydrogel incorporating PCL microspheres. Int J Pharm. 2018;537:278–89.
28. Chen X, Peng LH, Shan YH, Li N, Wei W, Yu L, et al. Astragaloside IV-loaded nanoparticle-enriched hydrogel induces wound healing and anti-scar activity through topical delivery. Int J Pharm. 2013;447:171–81.
29. Kaur P, Sharma AK, Nag D, Das A, Datta S, Ganguli A, et al. Novel nano-insulin formulation modulates cytokine secretion and remodeling to accelerate diabetic wound healing. Nanomedicine 2019;15:47–57.
30. Yu JS, Wang MY, Tai HC, Cheng NC. Cell sheet composed of adipose-derived stem cells demonstrates enhanced skin wound healing with reduced scar formation. Acta Biomater. 2018;77:191–200.
31. Luo P, Li XJ, Ye YJ, Shu X, Gong JJ, Wang JP. Castanea mollissima shell prevents an over expression of inflammatory response and accelerates the dermal wound healing. J Ethnopharmacol. 2018;220:9–15.
32. Kant V, Gopal A, Pathak NN, Kumar P, Tandan SK, Kumar D. Antioxidant and anti-inflammatory potential of curcumin accelerated the cutaneous wound healing in streptozotocin-induced diabetic rats. Int Immunopharmacol. 2014;20:322–30.
33. Feng ZT, Zhou HT, Ma SR, Guan XX, Chen LL, Huang J, et al. FTY720 attenuates intestinal injury and suppresses inflammation in experimental necrotizing enterocolitis via modulating CXCL5/CXCR2 axis. Biochem Biophys Res Commun. 2018;505:1032–7.
34. Herter EK, Li DQ, Toma MA, Vij M, Li X, Visscher D, et al. WAKMAR2, a long noncoding RNA downregulated in human chronic wounds, modulates keratinocyte motility and production of inflammatory chemokines. J Invest Dermatol. 2019;139:1373–84.
35. Lindley LE, Stojadinovic O, Pastar I, Tomic-Canic M. Biology and biomarkers for wound healing. Plast Reconstr Surg. 2016;138:18–28.
36. Orgul D, Eroglu H, Hekimoglu S. Formulation and characterization of tissue scaffolds containing simvastatin loaded nanostructured lipid carriers for treatment of diabetic wounds. J Drug Deliv Sci Technol. 2017;41:280–92.
37. Gokce EH, Tanrıverdi ST, Eroglu I, Tsapis N, Gokce G, Tekmen I, et al. Wound healing effects of collagen-laminin dermal matrix impregnated with resveratrol loaded hyaluronic acid-DPPC microparticles in diabetic rats. Eur J Pharm Biopharm. 2017;119:17–27.
38. Xu R, Bai Y, Zhao J, Xia HS, Kong Y, Yao ZH, et al. Silicone rubber membrane with specific pore size enhances wound regeneration. Tissue Eng Regen Med. 2018;12:905–17.
39. Chwalek K, Tsurkan MV, Freudenberg U, Werner C. Glycosaminoglycan-based hydrogels to modulate heterocellular communication in in vitro angiogenesis models. Sci Rep. 2014;4:4414. https://doi.org/10.1038/srep04414.
40. Li XL, Ye XL, Qi JY, Fan RR, Gao X, Wu YZ, et al. EGF and curcumin co-encapsulate nanoparticle/hydrogel system as potent skin regeneration agent. Int J Nanomed. 2016;11:3993–4009.
41. Tan KT, McGrouther DA, Day AJ, Milner CM, Bayat A. Characterization of hyaluronan and TSG-6 in skin scarring: differential distribution in keloid scars, normal scars and unscarred skin. J Eur Acad Dermatol. 2011;25:317–27.
42. Suarez E, Syed F, Rasgado TA, Bayat A. Identification of biomarkers involved in differential profiling of hypertrophic and keloid scars versus normal skin. Arch Dermatol Res. 2015;307:115–33.
43. Xu HL, Chen PP, Wang LF, Tong MQ, Ou ZH, Zhao YZ, et al. Skin-permeable liposome improved stability and permeability of bFGF against skin of mice with deep second degree scald to promote hair follicle neogenesis through inhibition of scar formation. Colloid Surf B. 2018;172:573–85.